PERGAMON

International Journal of Heat and Mass Transfer 42 (1999) 3609–3618

International Journal of HEAT and MASS TRANSFER

www.elsevier.com/locate/ijhmt

Improving the performance of double-pipe heat exchangers by using porous substrates

M.K. Alkam*, M.A. Al-Nimr

Mechanical Engineering Department, Jordan University of Science and Technology, Irbid, Jordan

Received 18 June 1998; received in revised form 30 December 1998

Abstract

This work introduces a novel method that improves the thermal performance of a conventional concentric tube heat exchanger. The introduced method includes inserting porous substrates at both sides of the inner tube wall. The porous substrates improve the convective heat transfer coefficient between the tube wall and the fluid. This improvement is investigated numerically and its effects on the effectiveness of the heat exchanger are evaluated. The present numerical results show that inserting the porous substrate may enhance the heat exchanger effectiveness considerably for both parallel flow and counter flow arrangements, especially at high values of the heat capacity ratios. In the current study, the effect of inserting porous substrates on the pumping head of the fluid is also investigated.

1. Introduction

The heat exchanger industry has been seeking ways to reduce the size and cost of heat exchangers. The enhancement of heat transfer has become an important factor in achieving these goals and has captured the interest of many researchers. Recent overviews of single phase tube enhancements are reported by Ravigururajan and Rabas [1], and Bergles [2]. Also, comprehensive assessments of enhancement options have bene published by Bergles [3], Webb et al. [4] and Webb [5]. Enhancement of heat transfer in heat exchangers can be accomplished through two techniques:

1. Increasing the convection coefficient. The convection coefficient may be increased by enhancing turbulence, creating secondary flow, and inducing swirl flow. One or more of these mechanisms may be accomplished using coil-spring wire, ribs, indentation, spiral flutes [5,6], transverse-ribbed tubes, helically ribbed tubes, wire-coil insert, twisted-tape insert [2], ribbed or ribbed grooved walls [7]. Also, the convective heat transfer coefficient may be enhanced using fluids that undergo a phase transition or by using electrohydrodynamic enhancement tools [8] and using mist flow [9].
2. Increasing the heat transfer area by using longitudinal fins [10], wire-on-tube heat exchangers [11].

Other techniques utilize both effects. Examples of these techniques are spiral fins or ribs and offset strip fins [2].

In the present work, it is intended to investigate numerically the effect of inserting porous substrates at both sides of the wall that separates the cold and hot working fluids on the performance of the heat exchanger. Previous studies showed that the heat transfer process in closed channels can be enhanced by partially

* Corresponding author. Tel.: +962 2 295 111; fax: +962 2 295 123.

E-mail address: malnimr@just.edu.jo (M.K. Alkam)

0017-9310/99/$ - see front matter
PII: S0017-9310(99)00033-2

Nomenclature

A	coefficient of the microscopic inertia term, $\epsilon Fr_2/\rho_R\sqrt{K}$
A_i	heat exchanger inner surface area, m^2
A_o	heat exchanger outer surface area, m^2
c_1	fluid specific heat
c_2	solid matrix specific heat
Da	Darcy number, K/r_2^2
F	Forchheimer coefficient
h	convective heat transfer coefficient
k	heat exchanger wall thermal conductivity
k_R	thermal conductivity ratio, k_2/k_1
k_1	fluid thermal conductivity
k_2	effective thermal conductivity in the porous domain
K	permeability of the porous substrate
$\dot{m}_A$	mass flow rate in channel A
$\dot{m}_B$	mass flow rate in channel B
N_1	dimensionless radius ratio, r_1/r_2
$N_2=1$	dimensionless radius ratio, $r_2/r_2=1$
N_3	dimensionless radius ratio, r_3/r_2
N_4	dimensionless radius ratio, r_4/r_2
Nu	local Nusselt number, $hr_2/k_2=(\partial\theta_2/\partial R)/(\theta_m-1)$
Nu_R	the value of Nusselt number with porous substrate divided by Nusselt number without porous substrate, $Nu_{with}/Nu_{without}$
p	pressure
P	dimensionless pressure, $pr_2^2/\rho_1\nu_1^2$
P_R	the value of fully developed pressure gradient with porous substrate divided by the fully developed pressure gradient without porous substrate, $(dP/dz_{with})/(dP/dZ_{without})$
Pr_1	Prandtl number of the fluid, $c_1\mu_1/k_1$
r	radial coordinate
r_1	inner radius of the inner porous substrate
r_2	radius of the inner tube (channel A)
r_3	outer radius of the outer porous substrate
r_4	radius of the outer tube (channel B)
R	dimensionless radial coordinate, r/r_2
T	temperature at any point
$T_{i,A}$	fluid inlet temperature to channel A
$T_{i,B}$	fluid inlet temperature to channel B
T_m	mixing cup temperature over any cross section
u	axial velocity
u_0	inlet axial velocity
U	dimensionless volume averaged axial velocity, ur_2/ν_1
U_0	dimensionless inlet axial velocity, u_0r_2/ν_1
UA	overall heat transfer coefficient
v	radial velocity
V	dimensionless radial velocity, vr_2/ν_1
z	axial coordinate
Z	dimensionless axial coordinate, z/r_2

Greek symbols

ϵ	porosity
$\bar{\epsilon}$	heat exchanger effectiveness
θ	dimensionless temperature, $(T-T_i)/T_i$
θ_m	dimensionless mixing cup temperature, $(T_m-T_i)/T_i$

μ_R	dynamic viscosity ratio, μ_2/μ_1
μ_1	fluid dynamic viscosity
μ_2	effective dynamic viscosity of the porous domain
ν	kinematic viscosity
ν_R	kinematic viscosity ratio, ν_2/ν_1
ρ	density
ρ_R	density ratio, ρ_2/ρ_1

Subscripts

A and B	channel A and B of the heat exchanger
R	ratio
s	solid matrix properties
ss	steady state
1 or f	fluid domain properties
2	porous domain properties

filling the channels with porous materials [12]. The aim of the present work is to improve the performance of the conventional concentric tube heat exchangers. This can be accomplished by inserting high-thermal conductivity porous substrates on both sides of the inner tube wall. A mathematical model is constructed to simulate the system under consideration. This model is used to study the effect of several operating and design parameters on the thermal performance of the heat exchanger.

2. Analysis

Consider a concentric tube heat exchanger as shown in Fig. 1. Two porous substrates are deposited at both sides of the inner tube. The velocity of the fluid at the entrance of the exchanger is kept uniform and steady $u_{o,A}$ and $u_{o,B}$, where subscripts A and B refer to the inner and outer tubes, respectively. In order to facilitate the solution of the governing equations, several assumptions are adopted. These assumptions include:

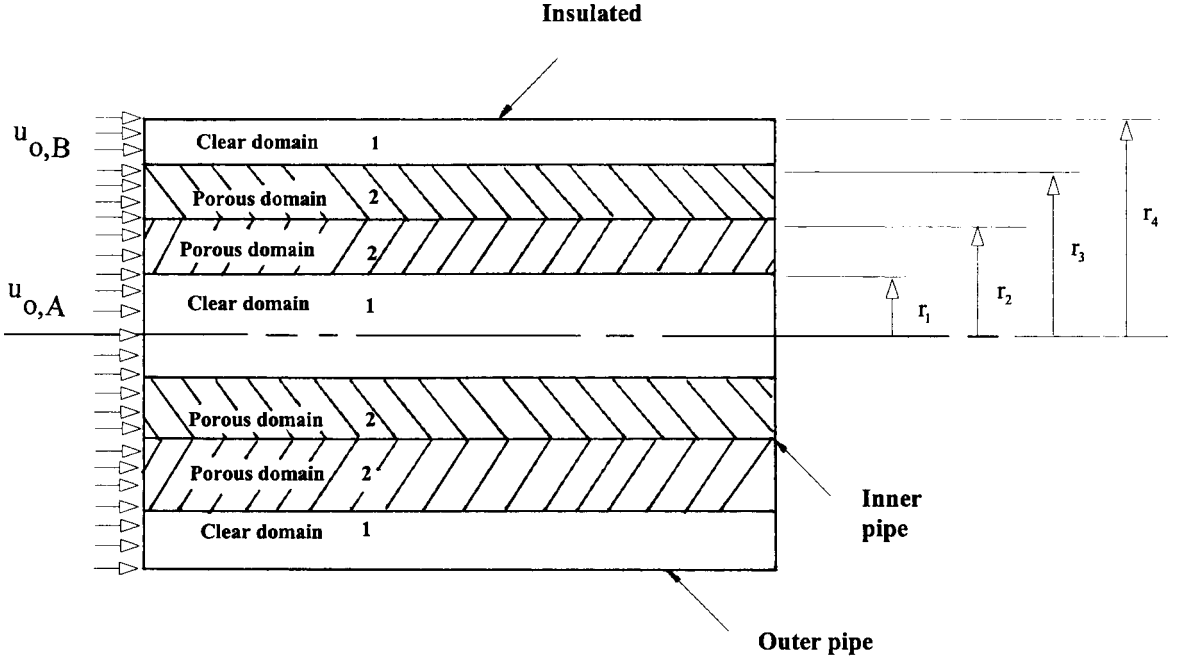

Fig. 1. Schematic diagram of a double-pipe heat exchanger.

1. axisymmetric flow, 2. laminar, boundary-layer flow with no internal heat generation, 3. no viscous dissipation, 4. no axial conduction of heat, and the wall thermal effects are neglected, 5. the porous medium is homogeneous, isotropic, and saturated with a single-phase fluid, 6. both the fluid and the solid matrix have constant physical properties, and 7. the solid matrix and the fluid are assumed to be at local thermal equilibrium with each other. The interactions between the porous medium and the clear fluid is simulated by the Darcy–Brinkman–Forchheimer formulation and the continuity of velocity and stresses at the interface [13]. Using the dimensionless parameters given in the nomenclature, the equations of continuity, motion, and energy, for both fluid and porous domains, in both inner and outer channels, are reduced to the following non-dimensional equations, respectively,

$$\frac{\partial U_1}{\partial Z}+\frac{1}{R}\frac{(R\,\partial V_1)}{2R}=0 \tag{1}$$

$$\frac{\partial U_2}{\partial Z}+\frac{1}{R}\frac{(R\,\partial V_2)}{\partial R}=0 \tag{2}$$

$$U_1\frac{\partial U_1}{\partial Z}+V_1\frac{\partial U_1}{\partial R}=-\frac{\partial P}{\partial Z}+\frac{1}{R}\frac{\partial}{\partial R}\left[R\frac{\partial U_1}{\partial R}\right] \tag{3}$$

$$U_2\frac{\partial U_2}{\partial Z}+V_2\frac{\partial U_2}{\partial R}=-\frac{1}{\rho_R}\frac{\partial P}{\partial Z}+\frac{\nu_R}{R}$$

$$\frac{\partial}{\partial R}\left[R\frac{\partial U_2}{\partial R}\right]-\frac{1}{\rho_R\,Da}U_2-AU_2^2 \tag{4}$$

$$U_1\frac{\partial \theta_1}{\partial Z}+V_1\frac{\partial \theta_1}{\partial R}=\frac{1}{Pr_1}\frac{1}{R}\frac{\partial}{\partial R}\left[R\frac{\partial \theta_1}{\partial R}\right] \tag{5}$$

$$U_2\frac{\partial \theta_2}{\partial Z}+V_2\frac{\partial \theta_2}{\partial R}=\frac{k_R}{Pr_1}\frac{1}{R}\frac{\partial}{\partial R}\left[R\frac{\partial \theta_2}{\partial R}\right] \tag{6}$$

In Eqs. (1)–(6), subscripts 1 and 2 refer to the clear fluid and porous substrate, respectively. The governing equations are solved by the linearized finite difference scheme of Bodoia and Osterle [14]. In the case under consideration, the momentum equations assume the following boundary conditions:

at $Z=0$ and $0<R<1$:

$$U_1=U_2=U_{o,A}\quad\text{and}\quad V_1=V_2=0$$

at $Z=0$ and $1<R<N_4$:

$$U_1=U_2=U_{o,B}\quad\text{and}\quad V_1=V_2=0$$

for $Z>0$ and $R=1$ (on both sides of the inner tube wall):

$$U_2=V_2=0$$

for $Z>0$ and $R=0$:

$$\frac{\partial U_1}{\partial R}=0$$

for $Z>0$ and $R=N_4$:

$$U_1=V_1=0$$

for $Z>0$ and $R=N_1$:

$$U_{1,A}=U_{2,A},\quad \frac{\partial U_{1,A}}{\partial R}=\mu_{R,A}\frac{\partial U_{2,A}}{\partial R}$$

for $Z>0$ and $R=N_3$:

$$U_{1,B}=U_{2,B},\quad \frac{\partial U_{1,B}}{\partial R}=\mu_{R,B}\frac{\partial U_{2,B}}{\partial R} \tag{7}$$

The energy equations have the following boundary conditions:

$$\text{at } R=0:\quad \frac{\partial \theta_1}{\partial R}=0$$

and at $R=1$ (on both sides of the inner tube wall):

$$\theta_2=(\theta_{i,A}+\theta_{o,A}+\theta_{i,B}+\theta_{o,B})/4=\theta_w \tag{8}$$

$$\text{at } Z=0,\quad 0<R<1:\quad \theta_{1,A}=\theta_{2,A}=\theta_{i,A}$$

$$\text{at } Z=0,\quad 1<R<N_4:\quad \theta_{1,B}=\theta_{2,B}=\theta_{i,B}$$

$$\text{at } Z>0,\quad R=N_1:\quad \theta_{1,A}=\theta_{2,A}\quad\text{and}\quad \frac{\partial \theta_{1,A}}{\partial R}=k_{R,A}\frac{\partial \theta_{2,A}}{\partial R}$$

$$\text{at } Z>0,\quad R=N_3:\quad \theta_{1,B}=\theta_{2,B}\quad\text{and}\quad \frac{\partial \theta_{1,B}}{\partial R}=k_{R,B}\frac{\partial \theta_{2,B}}{\partial R}$$

$$\text{at } Z>0,\quad R=N_4:\quad \frac{\partial \theta_{1,B}}{\partial R}=0 \tag{9}$$

In Eqs. (9), it is assumed that the wall of the outer tube is insulated. Also, it is assumed that the wall of the inner tube has negligible thermal effect and as a result, its inner and outer sides have the same temperature which is a uniform temperature θ_w given as the average of the inlet and outlet fluid temperatures entering and leaving both channels A and B. The last

assumption is used only in the process of estimating the convective heat transfer coefficient on both sides of the inner tube wall and it will not be used in the process of estimating the heat exchanger effectiveness. This is justified because the convective heat transfer coefficient is a weak function of the wall thermal conditions. However, this is not the case regarding the effectiveness. Also, it is worth mentioning that the above list of boundary conditions are given for the case of parallel flow heat exchanger and they are easily modified to include the counter flow arrangement. However, it is found that changing the flow arrangement from parallel to counter flow arrangement has negligible effect on the convective heat transfer coefficient on both sides of the inner tube wall. This is due to the assumption that the convective coefficient is a weak function of the wall thermal conditions, which is the only varying parameter after changing the exchanger arrangement.

3. Code validation and error estimates

A FORTRAN code has been constructed to solve the governing equations above by the finite difference scheme introduced by Bodoia and Osterle [14]. In order to validate the present code, two special runs were carried out corresponding to two special test cases. The first test case resembles the fully developed fluid flow through a pipe completely filled with porous material where both the microscopic and macroscopic inertia terms are neglected. In this case an analytical solution of the velocity profile is obtained. Eq. (10) below gives the closed form solution for the velocity profile for this special test case.

$$U_2(R) = Da\frac{U_0}{2\,Da\left(\dfrac{I_1(b)}{bI_0(b)} - \dfrac{1}{2}\right)}\left\{\frac{I_0(bR)}{I_0(b)} - 1\right\} \tag{10}$$

where $b = (1/\sqrt{\nu_R \rho_R\, Da})$. Fig. 2 shows a comparison between the analytical solution and the solution obtained by the present code for the fully developed velocity profile for the first test case. The second test case included the temperature distribution in a pipe completely filled with porous material. In this case, the flow is described by the plug flow model. The temperature distribution is obtained analytically as:

$$\theta_2(R, Z) = \sum_{n=1}^{\infty} \frac{2}{\gamma_n J_1(\gamma_n)} J_0(\gamma_n R)\, e^{-\gamma_n^2 \beta Z} \tag{11}$$

where $\beta = (k_R/Pr_1\ U_0)$, and γ_n are the roots of $J_0(\gamma_n) = 0$. The temperature profile obtained analytically [Eq. (11)] is compared with that calculated by the present code in Fig. 3. In order to obtain a solution that is independent of the grid size, several runs were performed with different grid sizes. An error parameter is defined as the absolute value of the temperature obtained by the present code minus the temperature obtained analytically for the second test case [Eq. (11)]. This error is calculated at each grid point over a prescribed cross section. The maximum local error is considered as a measure of the accuracy of the computations. For a radial step size $\Delta R = 0.01$, several runs were carried out for different values of axial step size

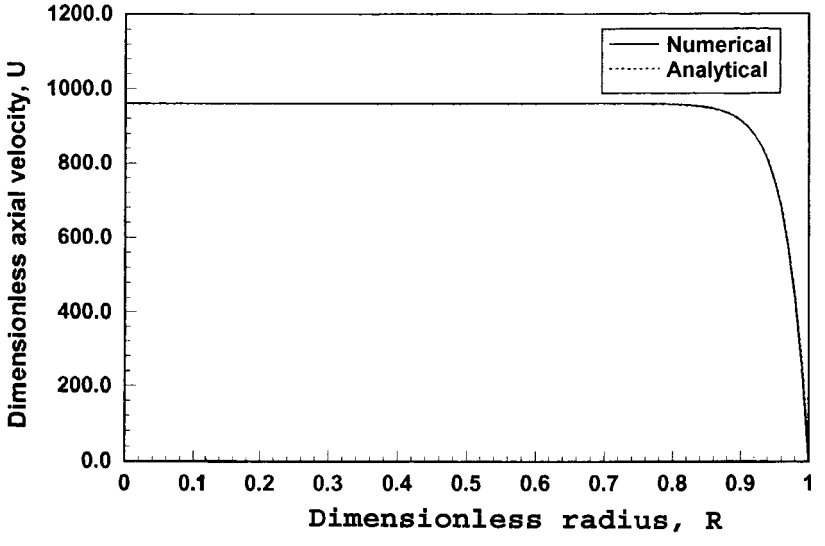

Fig. 2. Fully developed, non-dimensional axial velocity profile for the first test case. Comparison between present code and analytical solution.

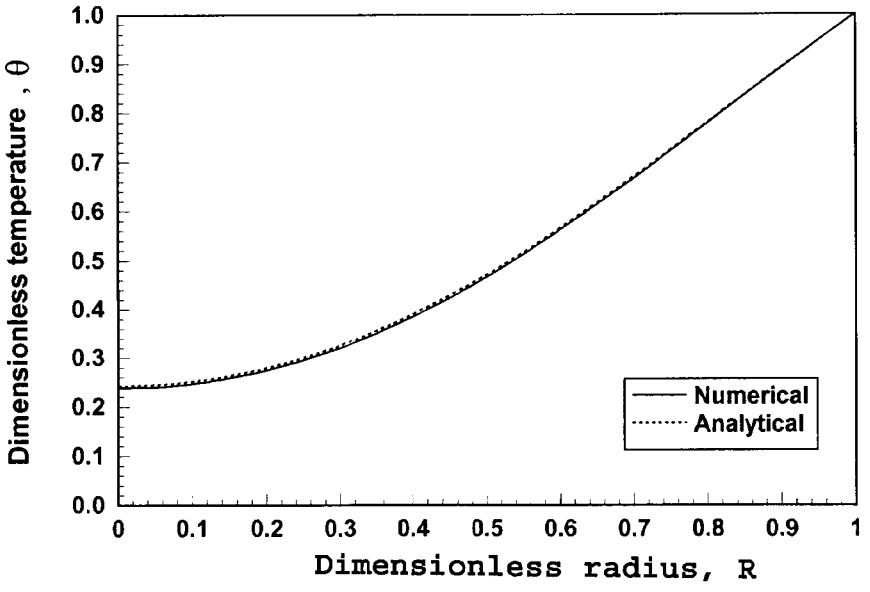

Fig. 3. Dimensionless temperature profile at $Z=10$ for the second test case. Comparison between present code and analytical solution.

ΔZ. For each run, the maximum error is calculated and tabulated in Table 1. The optimum choice for ΔZ was 0.1. Similarly, several runs were carried out corresponding to different values of ΔR, keeping ΔZ at 0.1. The results are shown in Table 2 where the optimum choice was $\Delta R=0.02$.

4. Effect of the porous substrate thickness on the convective heat transfer coefficient

Using the appropriate dimensionless operating conditions, Eqs. (1)–(9) are solved numerically after validating the used computer code to find the Nusselt number, *Nu*, at both sides of the inner tube wall. For each set of operating conditions, the *Nu* number at both sides of the wall is evaluated twice; with and without porous substrate. The effects of the porous substrate thicknesses $1-N_1$ (thickness of the inner substrate) and N_3-1 (thickness of the outer substrate) on the value of Nu_R (*Nu* with porous substrate/*Nu* without porous substrate) at both sides of the wall are shown in Fig. 4, for the following dimensionless operating conditions that represent water as the working fluid and an aluminum matrix as the porous domain. Aluminum is considered a typical high thermal conductivity material. The value of $\mu_{R,A}=\mu_{R,B}=1.0$. This choice of the viscosity ratio is recommended by Kakac et al. [15].

$$Pr_{l,A}=Pr_{l,B}=7.0,\quad k_{R,A}=K_{R,B}=78.12,$$

$$\mu_{R,A}=\mu_{R,B}=1.0,\quad \rho_{R,A}=\rho_{R,B}=2.7$$

$$U_{o,A}=300,\quad U_{o,B}=900,\quad N_4=2,\quad \theta_{i,A}=\theta_{i,B}=0,$$

$$Da=0.001,\quad A=1.0$$

As shown from this figure, increasing the substrate thickness improves the fully developed *Nu* number up to 100 times on the inner side of the wall and up to 80 times on the outer side of the wall. Also, the effect of the substrate thickness on the pressure drop ratio P_R, in both channels of the heat exchanger, is shown in Fig. 5 for the same set of operating conditions. Due to its high macroscopic and microscopic shear, bulk and

Table 1
Effect of the axial step size (ΔZ) on the maximum error, $\Delta R=0.01$

ΔZ	10	5	1	0.5	0.1	0.05
Error	8.78e-2	4.18e-2	8.32e-3	4.34e-3	1.26e-3	8.4e-4

Table 2
Effect of the radial step size (ΔR) on the maximum error, $\Delta Z=0.1$

ΔR	0.1	0.05	0.025	0.02	0.01
Error	2.02e-2	5.02e-3	1.58e-3	1.41e-3	1.26e-3

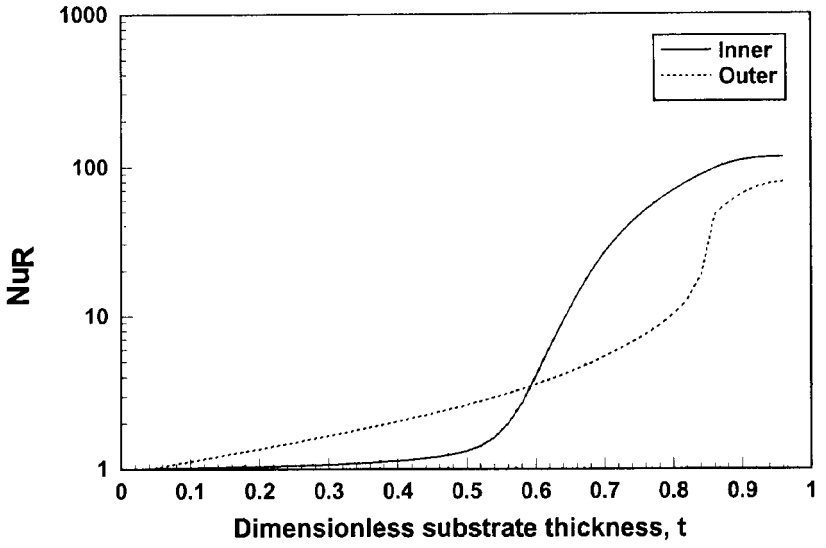

Fig. 4. Effect of substrate thickness on the improvement in Nusselt number for both the inner and outer sides of the inner tube.

microscopic inertial drag forces, the porous substrate has the effect of increasing the pressure drop within both the inner and outer tubes. As a result, higher pumping work is required to maintain the same amount of flow rate if the substrate thickness is increased.

5. Thermal performance of the modified heat exchanger

The performance of the heat exchanger is usually quantified in terms of its effectiveness which is defined as:

$$\bar{\epsilon} = \frac{q}{q_{\max}} = \frac{q}{C_{\min}(T_{h,i} - T_{c,i})} \tag{12}$$

where q is the actual rate of heat transfer in the heat exchanger, $q_{\max}$ is the maximum possible heat transfer rate, $C_{\min}$ is $\dot{m}_c c_c$ or $\dot{m}_h c_h$ whichever is smaller, T_h and T_c are the temperatures of the hot and cold streams, respectively.

For concentric tubes heat exchangers, the effectiveness is given as [16]:

For parallel flow heat exchanger:

$$\bar{\epsilon} = \frac{1 - e^{-NTU(1+C_r)}}{1 + C_r} \tag{13}$$

and for counter flow heat exchanger:

$$\bar{\epsilon} = \frac{1 - e^{-NTU(1-C_r)}}{1 - C_r e^{-NTU(1-C_r)}} \tag{14}$$

where

$$C_r = \frac{C_{\min}}{C_{\max}}, \quad NTU = \frac{(UA)_i}{C_{\min}} = \frac{(UA)_o}{C_{\min}} \quad \text{and}$$

$$\frac{1}{UA} = \frac{1}{h_i A_i} + \frac{Ln\left(\frac{r_2 + \delta}{r_2}\right)}{2\pi k L} + \frac{1}{h_o A_o}$$

where δ is the thickness of the inner tube wall, L is the heat exchanger length, A_i and A_0 are the inner and outer surface areas of the inner tube.

The effects of the inner and outer porous substrates thickness on the heat exchanger effectiveness for parallel and counter flow arrangements are shown in Fig. 6. It is clear from these figures that inserting substrates of high thermal conductivity may improve the effectiveness considerably for parallel flow and counter flow arrangements. The percentage improvement, for the same substrate thickness, is lower in the counter flow arrangement since the effectiveness of the conventional counter flow heat exchanger is higher than that of the conventional parallel flow exchanger. Also, it is clear from these figures that there is a critical substrate thickness beyond which there is no further improvement in $\bar{\epsilon}$. This is due to the fact that any further increase in the substrate thickness will not affect the thermal behavior of the thin layer which is very near the wall that separates the hot and cold streams. The effect of the substrate thickness on $\bar{\epsilon}$ and for different C_r is shown in Figs. 7 and 8 for parallel and counter flow arrangement, respectively. As shown in these figures, increasing the substrate thickness, on both sides of the inner tube wall, has more significant improvement for large values of C_r. The ratio C_r may be decreased by decreasing $C_{\min}$, and as a result the number of transfer units NTU increases. Increasing the

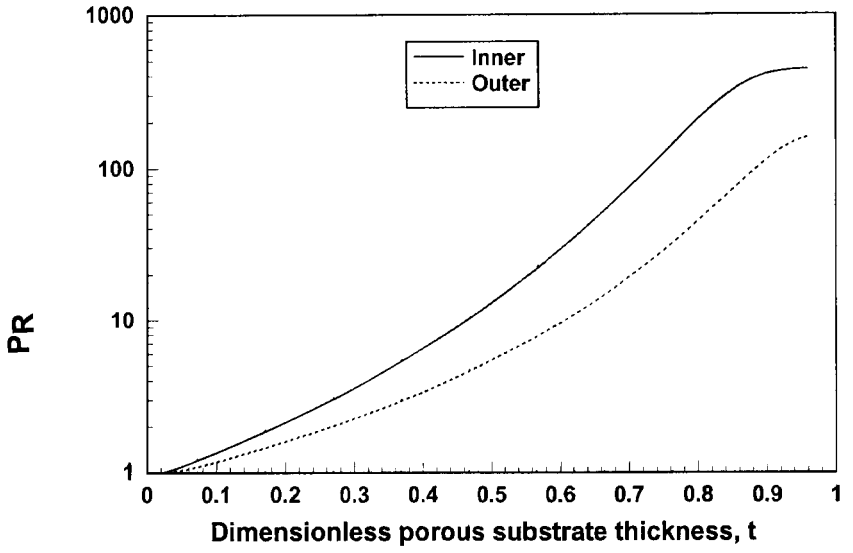

Fig. 5. Effect of substrate thickness on the fully developed pressure gradient for both the inner tube and the outer channel.

number of transfer units has the same effect as increasing the overall heat transfer coefficient U. As a result, increasing the substrate thickness in heat exchangers having high U has no significant improvement. In the limit as $C_r \to 0$ (as in boiling or condensation), the porous substrate thickness has no effect on $\bar{\varepsilon}$. In the case of boiling or condensation, $NTU \to \infty$, hence, UA is very large without inserting the porous substrate. Any improvement in UA is not significant. For the special case of $C_r \to 0$, the heat exchanger behavior is independent of flow arrangement. Fig. 9 shows the effect of the thermal conductivity ratio on the effectiveness of the heat exchanger for both parallel and counter flow arrangements. It is clear from the figure that increasing the thermal conductivity ratio enhances the heat transfer, and thus, improves the effectiveness of the heat exchanger.

6. Conclusions

In the present work, the thermal performance of a

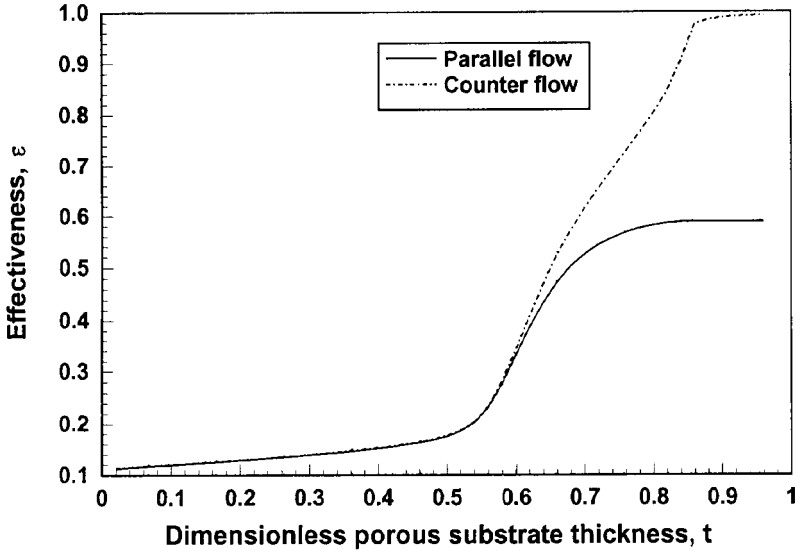

Fig. 6. Effect of the porous substrate thickness on the heat exchanger effectiveness for both counter flow and parallel flow arrangements. $C_r = 0.7$.

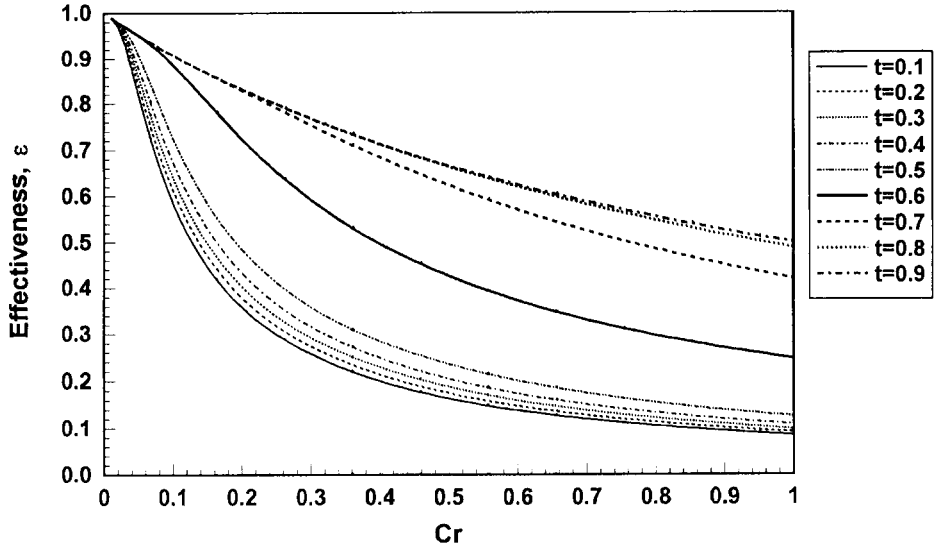

Fig. 7. Effect of C_r on the effectiveness of the parallel flow heat exchanger for different values of substrate thickness (t).

conventional heat exchanger is improved by inserting porous substrates at both sides of the inner tube wall. The porous substrates improve the convective heat transfer coefficient between the tube wall and the fluid. It is found that this improvement raises the effectiveness of the exchanger considerably for both parallel and counter flow arrangements. The improvement in the exchanger effectiveness is high especially at high values of the heat capacity ratios C_r. However, inserting the porous substrate has the effect of increasing the pressure drop within the heat exchanger. Also, it is found that there is a critical value of substrate thickness beyond which there is no substantial increase in the exchanger performance. Inserting substrates of

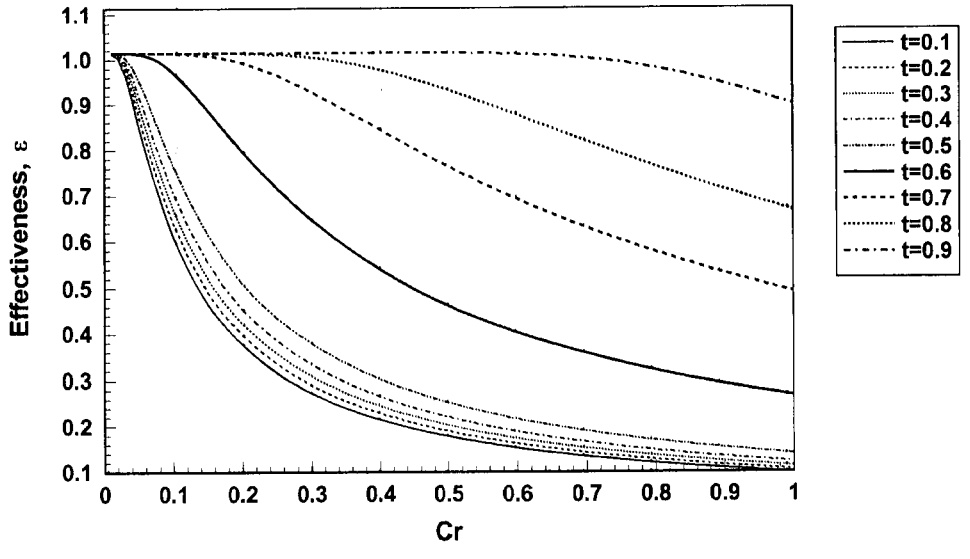

Fig. 8. Effect of C_r on the effectiveness of the counter flow heat exchanger for different values of substrate thickness (t).

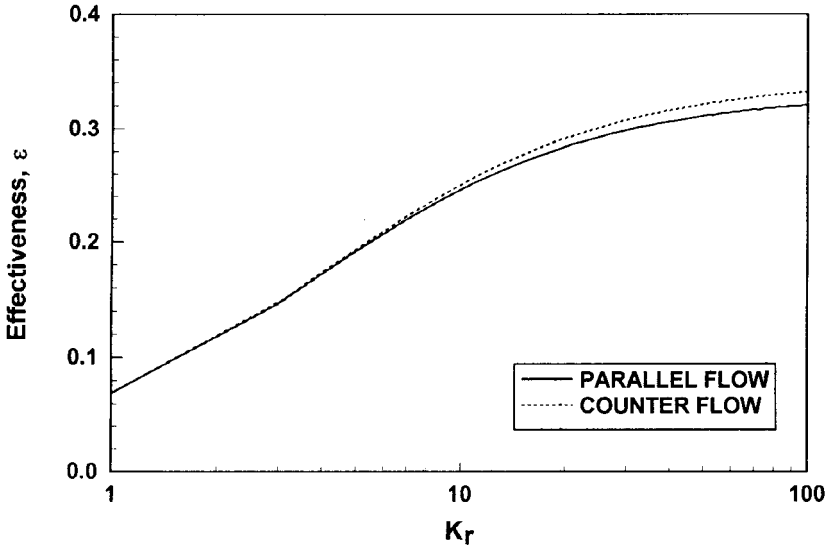

Fig. 9. Effect of the thermal conductivity ratio on the effectiveness of the heat exchanger for both parallel and counter flow arrangements. $C_r = 0.7$, and $t = 0.8$.

optimum thickness yields the maximum improvement in the exchanger thermal performance with moderate increase in its pumping cost.

References

[1] T.S. Ravigururajan, T.J. Rabas, An overview of single-phase in-tube enhancements: Part I—data-base development, ASME 93-WA/HT-38 (1993) 1–8.

[2] A.E. Bergles, Heat transfer enhancement—the taturing of second-generation heat transfer technology, Heat Transfer Engineering 18 (1) (1997) 47–55.

[3] A.E. Bergles, in: Principles of Heat Transfer Augmentation, Heat Exchangers, Thermal-Hydraulic Fundamentals and Design, Hemisphere, New York, 1981, pp. 819–842.

[4] R.L. Webb, S. Kakac, R.K. Shah, W. Aung (Eds.), Handbook of Single-Phase Convective Heat Transfer, Wiley-Interscience, New York, 1987.

[5] R.L. Webb, Principles of Enhanced Heat Transfer, Wiley, New York, 1994.

[6] D.D. Joye, A.S. Cote, Heat transfer enhancement in annular channels with helical and longitudinal fins, Heat Transfer Engineering 16 (2) (1995) 29–34.

[7] Y.M. Zhang, W.Z. Gu, J.C. Han, Heat transfer and friction in rectangular channels with ribber or ribbed-grooved walls, ASME J. Heat Transfer 116 (1994) 58–65.

[8] K. Yamashita, A. Yabe, Electrohydrodynamic enhancement of falling film evaporation heat transfer and its long-term effect on heat exchanges, ASME J. Heat Transfer 119 (1997) 339–347.

[9] S.L. Lee, Z.H. Yang, Y. Hsyua, Cooling of a heated surface by mist flow, ASME J. Heat Transfer 116 (1994) 167–172.

[10] J. Taborek, Double-pipe and multitube heat exchangers with plain and longitudinal finned tubes, Heat Transfer Engineering 18 (2) (1997) 34–45.

[11] J.L. Hoke, A.M. Clausing, T.D. Swofford, An experimental investigation of convective heat transfer from wire-on-tube heat exchangers, ASME J. Heat Transfer 119 (1997) 348–356.

[12] M.A. Al-Nimr, M. Alkam, Unsteady non-Darcian forced convection analysis in an annulus partially filled with a porous material, ASME J. Heat Transfer 119 (1997) 799–804.

[13] K. Vafai, S.J. Kim, On the limitations of the Brinkman–Forchheimer-extended Darcy equation, Int. J. Heat and Fluid Flow 16 (1995) 11–15.

[14] J.R. Bodoia, J.F. Osterle, Finite-difference analysis of plane Poiseuille and Couette flow developments, Appl. Sci. Res. A10 (1961) 265–276.

[15] S. Kakac, B. Kilkis, F. Kulacki, F. Arinc, in: Convective Heat and Mass Transfer in Porous Media, Kluwer, Netherlands, 1991, pp. 563–615.

[16] F. Incropera, D. DeWitt, Fundamentals of Heat and Mass Transfer, John Wiley and Sons, New York, 1996, Chap. 11.